AIAA 81-1288R

Dynamic Stall Due to Fluctuations of Velocity and Incidence

D. Favier,* C. Maresca,† and J. Rebont‡
Institut de Mécanique des Fluides, CNRS, Marseille, France

Proper simulation of a retreating-blade stall requires considering incidence fluctuations combined with simultaneous velocity oscillations of the incoming airstream. This paper reports experimental results obtained when simultaneous fluctuations of both velocity and incidence are generated on an airfoil executing oblique fore-and-aft translations. When dynamic stall occurs in out-of-phase or in-phase variations of incidence and velocity, strong unsteady effects are present. In the first case, an instantaneous lift overshoot and a time delay between incidences of dynamic and static stall are observed. In the second case, the main effect consists of an overshoot of the mean aerodynamic coefficients over the period, owing to a cyclic separation and reattachment process with a strong vortex shedding all along the upper surface during the separation phase.

Nomenclature

A	= amplitude of oscillation, m
c	= airfoil chord, m
C_L	= lift coefficient, $C_L = L/\frac{1}{2}\rho V^2 ch$
C_D	= drag coefficient, $C_D = D/\frac{1}{2}\rho V^2 ch$
C_M	= moment coefficient, $C_M = M/\frac{1}{2}\rho V^2 c^2 h$
f	= frequency of oscillation, Hz
h	= airfoil span, m
k	= frequency parameter, $k = c\omega/2V_\infty$
Re	= Reynolds number, $Re = V_\infty c/\nu$
T	= period of oscillation, s
t	= time, s
V_∞, V	= freestream and instantaneous velocities, m/s
α	= instantaneous incidence, deg
α_0	= geometric airfoil incidence, deg
α_{SS}, α_{DS}	= incidences for static and dynamic stall
δ	= angle of oscillation axis, deg
λ	= amplitude parameter, $\lambda = A\omega/V_\infty$
ν	= kinetic viscosity
ρ	= air density
τ, τ_{st}	= unsteady and steady shear stress
ω	= pulsation of oscillation, rad/s

Introduction

THE study of dynamic stall airfoils, which is of great interest in the basic understanding of aerodynamics, has given rise to active research effort during the past decade. This effort has been motivated[1,2] primarily by the unsteady flowfield through helicopter rotors, and specifically by the dynamic stall occurring on the retreating blade which is a limiting factor in rotor performance. Although proper simulation of the surrounding blade flow requires considering simultaneous velocity and incidence fluctuations, most of the studies undertaken on this problem have separated the influences of the various parameters by investigating unsteady flows over airfoils oscillating either in pitch[3-6] or in translation parallel or normal to the freestream direction.[7-10]

The focus of the present paper is to investigate the unsteady effects generated on an airfoil experiencing simultaneous fluctuations in both velocity and incidence. This new simulation of the problem is carried out by means of an oblique fore-and-aft motion of the airfoil, which allows variations of the instantaneous velocity and incidence, either in phase or out of phase. During dynamic stall, quite different unsteady flow features are observed in each case of out-of-phase or in-phase simulation. In the following sections the results obtained from these oblique airfoil motions will be discussed and compared with those already obtained in the cases of the single oscillating velocity (longitudinal motion) or of the single oscillating incidence (pitching and plunging motions).

Airfoil Motion and Simulation Conditions

As shown in Fig. 1a, the airfoil is set at a fixed incidence α_0 and is forced to oscillate in fore-and-aft translations of amplitude $\pm A$ and frequency f along the X_δ axis. The cyclic displacement of the airfoil along the X_δ oscillation axis is given by $x = A\sin\omega t$, so that simultaneous fluctuations of both relative velocity V and incidence α can be obtained according to the subsequent equations

$$V^2 = V_\infty^2 (1 + 2\lambda\cos\omega t\cos\delta + \lambda^2\cos^2\omega t)$$
$$\alpha = \alpha_0 - \text{arctg}\left[(\lambda\cos\omega t\sin\delta) / (1 + \lambda\cos\omega t\cos\delta) \right] \quad (1)$$

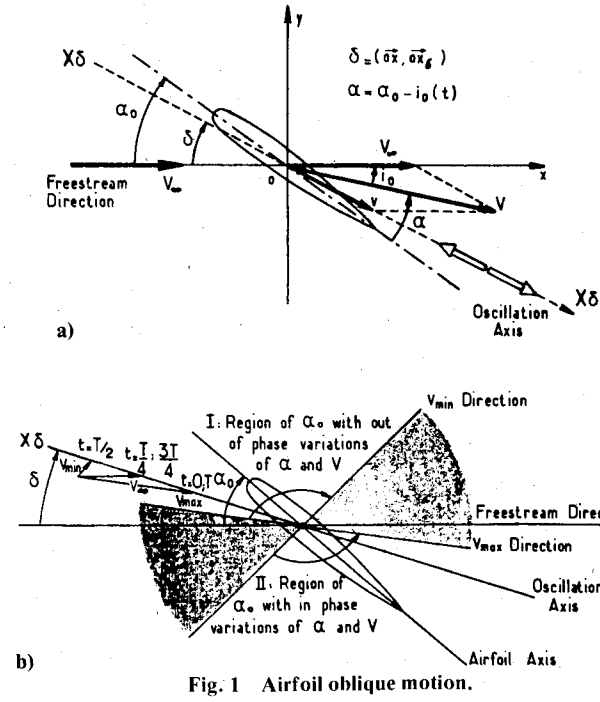

Fig. 1 Airfoil oblique motion.

Presented as Paper 81-1288 at the AIAA 14th Fluid and Plasma Dynamics Conference, Palo Alto, Calif., June 23-25, 1981; submitted July 16, 1981; revision received Nov. 12, 1981.

*Research Scientist. Member AIAA.
†Senior Research Scientist. Member AIAA.
‡Research Engineer.

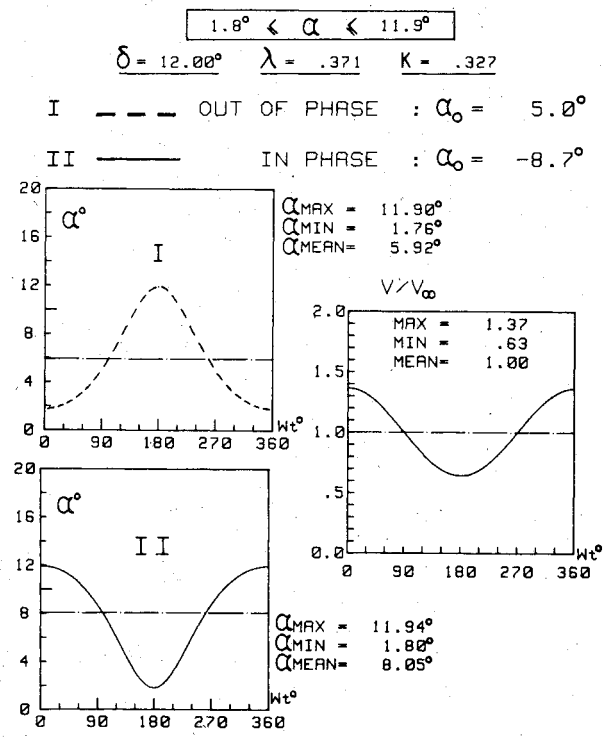

Fig. 2a V and α oscillations below stall.

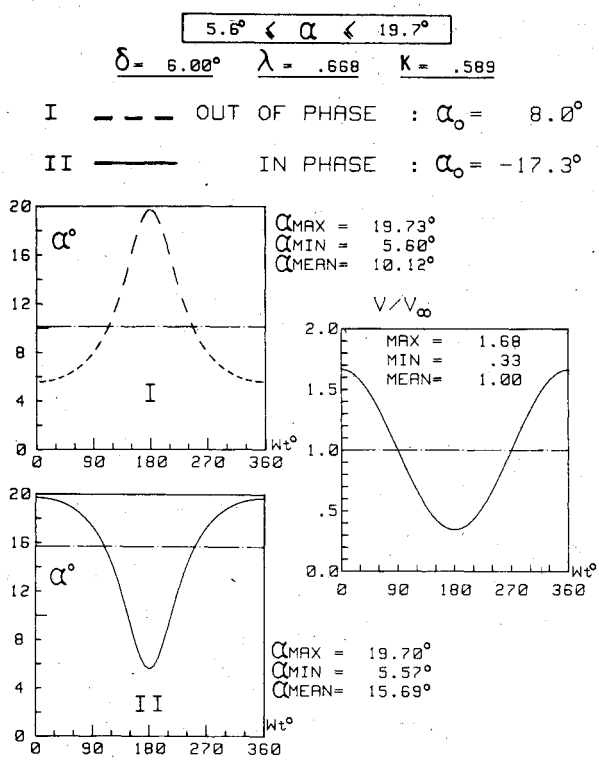

Fig. 2b V and α oscillations through stall.

By selecting appropriate values of the angles δ and α_0, the experimental setup simulates fluctuations of V and α, either in phase (when V_{max} is coinciding with α_{max}) or out of phase (when V_{max} is coinciding with α_{min}). During the first half of the cycle, the airfoil moves forward from its middle position at $t=0$ and $V=V_{max}$, reaches its maximum forward position at $t=T/4$ and $V=\bar{V}=V_\infty$, and then returns to its middle position at $t=T/2$ and $V=V_{min}$. During the second half of the cycle the airfoil is executing a symmetrical displacement and values of V_{min}, V_∞, and V_{max} are successively obtained for $t=T/2$, $3T/4$, and T.

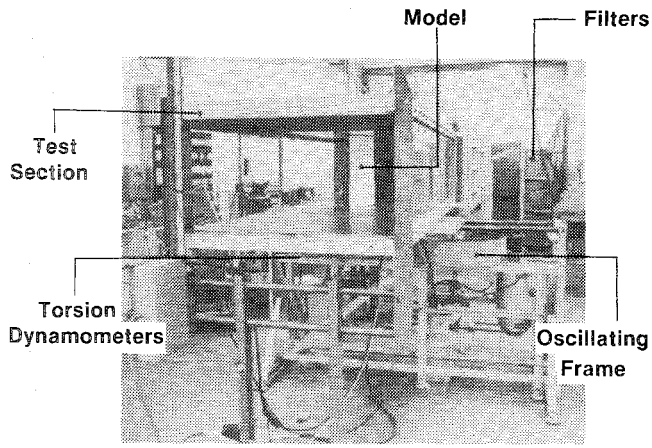

Fig. 3 View of the experimental setup.

From the above velocity fluctuations sketched in Fig. 1b, it can be seen that selecting α_0 in region I leads to an increase of the instantaneous incidence α during the first half cycle, and to a decrease of α during the second half (i.e., out-of-phase variations are obtained on V and α). In phase variations of V and α will be generated when α_0 is selected from region II.

Due to the symmetry of the airfoil, it can be noticed that negative values of α obtained from Eq. (1) when α_0 is chosen in region II can be expressed as positive α variations by considering a change of sign in the sense of forces and moments acting on the airfoil. As an example, Figs. 2a and 2b give the resulting out-of-phase and in-phase variations of V and α, obtained with appropriate couples of the δ and α_0 parameters. For $\delta=12$ deg, $\lambda=0.37$, and $k=0.33$ (Fig. 2a), out-of-phase or in-phase variations are generated with $\alpha_0=5$ or -8.7 deg, and the resulting instantaneous incidence α varies below the incidence of static stall ($\alpha_{SS}=12$ deg). For $\delta=6$ deg, $\lambda=0.67$, and $k=0.59$ (Fig. 2b), out-of-phase or in-phase variations are obtained with $\alpha_0=8$ or -17.3 deg, and the instantaneous incidence α varies through stall ($5.6 \text{ deg} < \alpha < 19.7$ deg).

Experimental Facilities and Procedures

Experiments are conducted in the IMFM low-turbulence open-circuit wind tunnel. The rectangular test section (0.5×1 m^2) is 3 m long (see Fig. 3). Under steady flow conditions the range of static Reynolds number is $5\times10^4 < Re < 4\times10^5$. The model consists of a rectangular wing spanning the entire test section (span $h=0.495$ m and chord $c=0.30$ m), with a NACA 0012 symmetrical profile of $\alpha_{SS}=12$ deg for angle of static stall incidence. As shown in Fig. 3 this airfoil is held vertically in the test section by two masts through a gap on the wall, which are attached on a frame oscillating sinusoidally in fore-and-aft translations. Due to the removal of the diffuser downstream of the test section (see Fig. 3) the static pressure along the walls of the test section is very nearly equal to the outside atmospheric pressure, so that there is no flow through the gap in the wall supporting the instrumented airfoil.

Amplitudes and frequencies of the oscillating frame can be varied in the ranges $0<A<0.17$ m and $0<f<5$ Hz, so that the reduced amplitude λ and the reduced frequency k are varied at 0-1.2 and 0-1.6, respectively.

The object of these tests is to simulate in the wind tunnel fluctuations of velocity and incidence around the airfoil. As is the case for the single oscillation of either velocity or incidence, the truly two-dimensional dynamic or even static stall remains difficult[11,12] to simulate without wind-tunnel or support interferences. As shown by experiments[13,14] carried out with and without slotted walls, it appears that the wind-tunnel corrections required for dynamic stall characteristics are significantly smaller than those required for static stall.

Moreover, in steady flow, these results[14] indicate that the maximal normal force coefficient at stall was either 7 or 2% higher than the exact value, when using either a closed tunnel or a slotted (2% open) sidewall in the test section.

Consequently, from the present experimental setup all of the results are given as two-dimensional data with no corrections made for any interference effects which might have been present. In steady flow the result concerning the stall angle and the maximum lift, drag, and moment are obviously related to the aerodynamic aspect ratio of the wing which is about 5 and with the range of Reynolds numbers used in the tests. However, in unsteady flow these interference effects are believed to be smaller,[14] and cannot affect significantly the dynamic characteristics of the discussed phenomena.

Measurements of aerodynamic forces and moments have been carried out by means of torsion dynamometers calibrated dynamically. Skin friction and static pressure distributions along the chordwise direction have been performed by nine hot-film skin friction gages and eight Kulite pressure transducers, mounted flush on the skin airfoil surface. Two models of the same wing have been equipped to measure surface pressure and skin friction distributions. On each model the row of hot films or of transducers is located in the midspan section of the wing. The gages are progressively spaced toward the trailing edge at $x/c=0.04$-0.8 and they are staggered along the centerline of the wing. The wake patterns around the model are revealed by a visualization technique based on the upstream emission of white smoke-filaments from a seven-tooth comb. The operating procedures for visualizations or forces, moments, skin friction, and pressure measurements are described in detail in Refs. 7-10.

All of the output signals from torsion dynamometers, skin friction gages, and pressure transducers were digitized and stored by an 800 channel data acquisition system. These data are then harmonically analyzed within a computer (HP 9845) to yield the time-averaged value and the four Fourier harmonics in the following form:

$$C=C_0+\sum_{n=1}^{4} C_n\cos(n\omega t+\phi_n) \qquad (2)$$

where C is the quantity to be measured and C_0 the mean value of C over the period of oscillation.

Although no significant data scattering has been observed during the tests, the following results of forces and moments were recorded on a 20 cycles averaging-signal procedure in order to improve the signal/noise ratio. For frequencies of oscillation up to 4 Hz, it appears that only four harmonics could be used in the Fourier series of Eq. (2) to represent the original record. The differences between the instantaneous and averaged signal remain within the error band of the measuring technique (less than 7%) with this procedure. Local pressure and skin friction measurements were carried out on a single time-history record at each probe location in order to detect the imprint made by the upper side vortex propagation.

Results and Discussion

Oscillation below Stall

The variations of lift, drag, and moment coefficients, deduced from the torsion-dynamometer averaging procedure, are presented in Figs. 4-6 as functions of the instantaneous incidence α varying in the range $1.8\ \text{deg}<\alpha<11.9\ \text{deg}$ and described in Fig. 2a for $\delta=12$ deg, $\lambda=0.37$, and $k=0.33$. The C_L, C_D, and C_M coefficients have been nondimensionalized by the instantaneous quantity $\frac{1}{2}\rho V^2 ch$ (or $\frac{1}{2}\rho V^2 c^2 h$ for the moment). In these figures out-of-phase (dotted line) and in-phase (full line) variations are also compared to the corresponding steady variations when α is varying within the limit of static stall ($\alpha<\alpha_{SS}$).

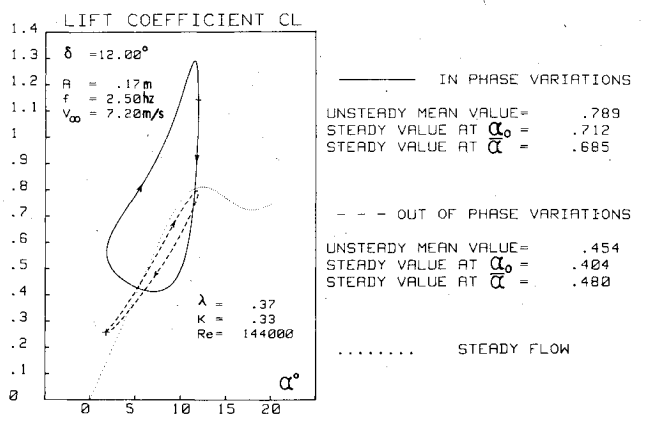

Fig. 4 C_L variations below stall.

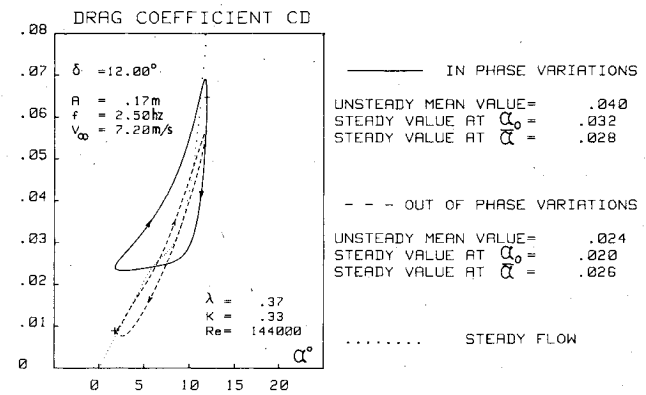

Fig. 5 C_D variations below stall.

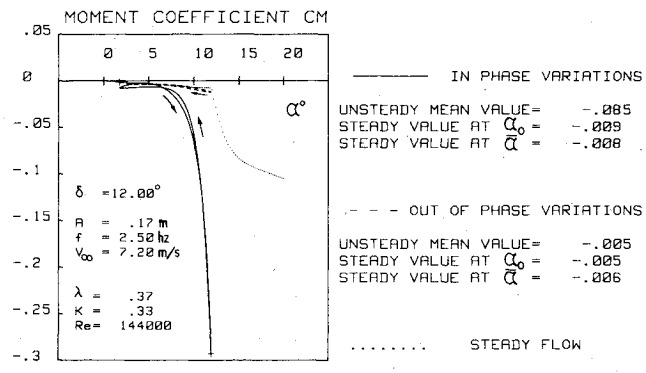

Fig. 6 C_M variations below stall.

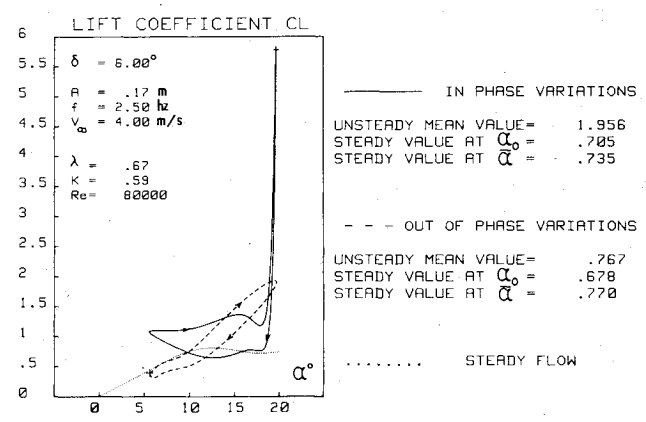

Fig. 7 C_L variations through stall.

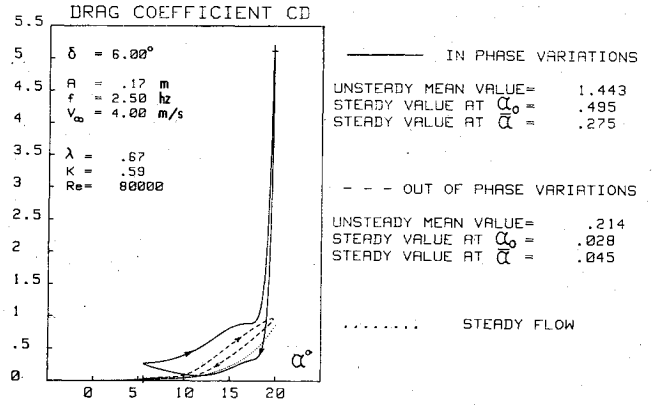

Fig. 8 C_D variations through stall.

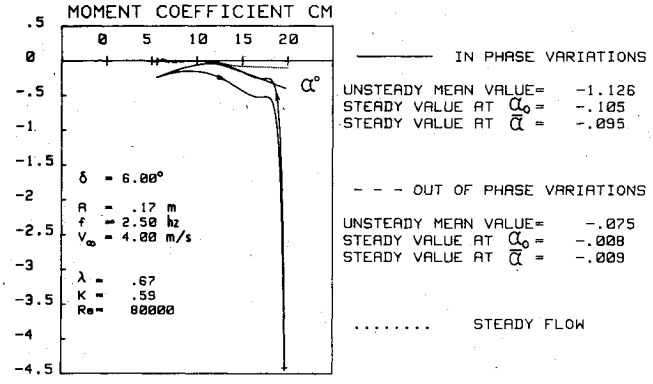

Fig. 9 C_M variations through stall.

When in-phase oscillations of V and α are simulated, it can be seen that lift, drag, and moment variations behave like the oscillations of velocity V/V_∞, which are also in this case those of incidence α (Fig. 2a). The maximum and minimum values of C_L, C_D, and C_M obtained at approximately the same phases ωt that the maximum and minimum values of the V and α oscillation, provide large amplitude fluctuations of forces and moment with an increase of the mean values of $\overline{C_L}$, $\overline{C_D}$, and $\overline{C_M}$ over the period. As an example, Fig. 4 clearly shows that the unsteady mean value over the period reaches a value $\overline{C_L}=0.789$, while values of C_L obtained in steady flow at the mean incidence ($\alpha=\bar{\alpha}=8$ deg, $V\sim\bar{V}$) and at the static incidence α_0 are 0.712 and 0.685, respectively.

On the other hand, when out-of-phase oscillations of V and α are simulated (dotted lines in Figs. 4-6), the forces and moment behave like the α oscillation (see Fig. 2a). The maximum lift is obtained in the same phase ($\omega t=180$ deg) as the maximum incidence, but the low velocity values ($V/V_\infty\sim0.63$) do not allow the instantaneous lift level to reach as high a level in the in-phase case. As indicated on Fig. 4 the lift behavior is close to the steady one, and no gain in the unsteady mean lift over the period is observed for this out-of-phase simulation. With the flow conditions of Fig. 4, the values of C_L measured in steady flow at α_0 and $\bar{\alpha}$ are 0.404 and 0.480, respectively, while the value of $\overline{C_L}$ is 0.454. For this last case, the hysteresis loops obtained on C_L, C_D, and C_M are quite similar to those previously obtained in the case of pure α oscillations generated by pitching[4-6] or plunging[9,10] motions.

As described below, the above behavior of forces and moments due to out-of-phase and in-phase variations of V and α, which is observed for an α oscillation below stall, becomes more accentuated when stall penetration occurs.

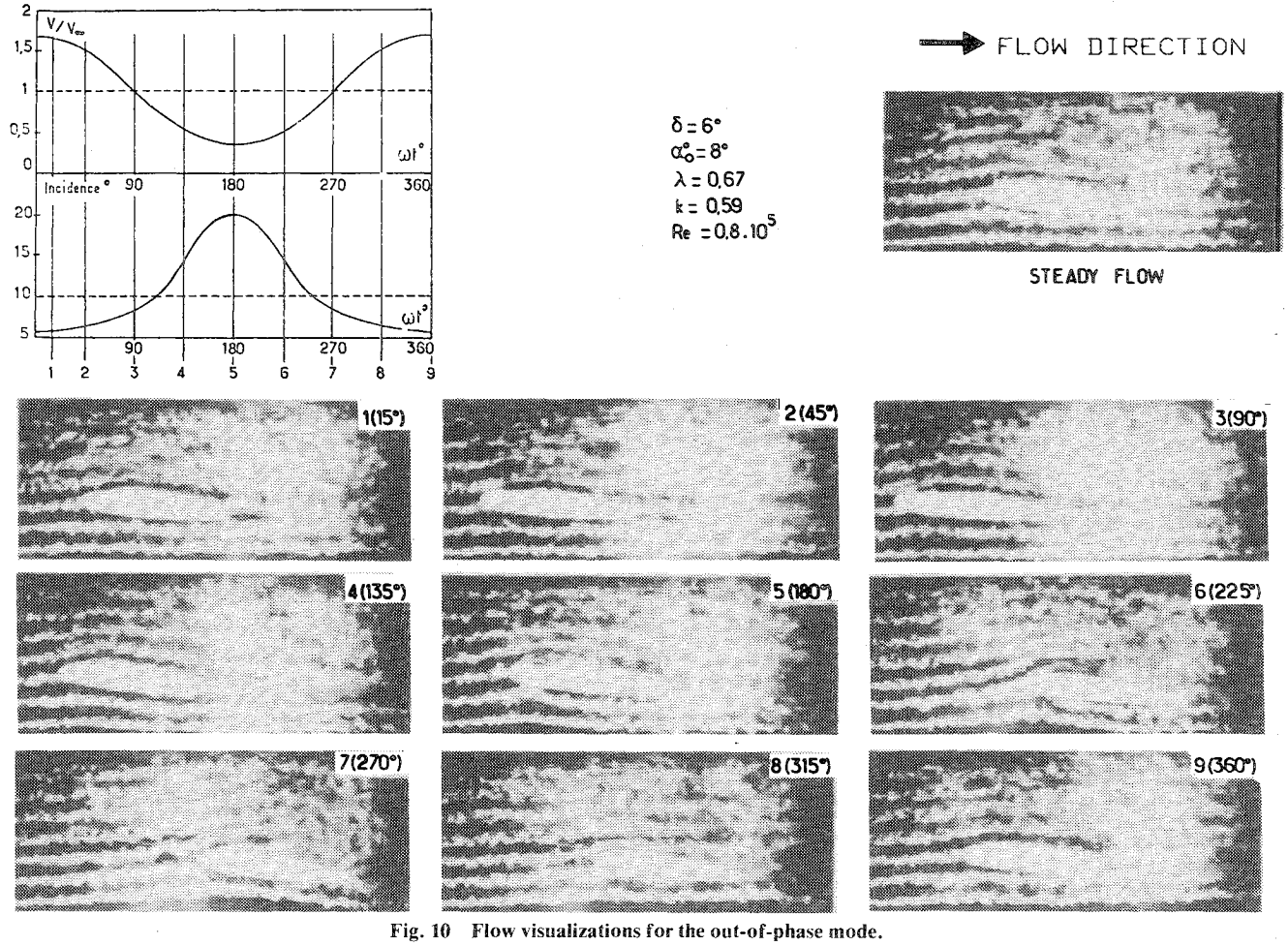

Fig. 10 Flow visualizations for the out-of-phase mode.

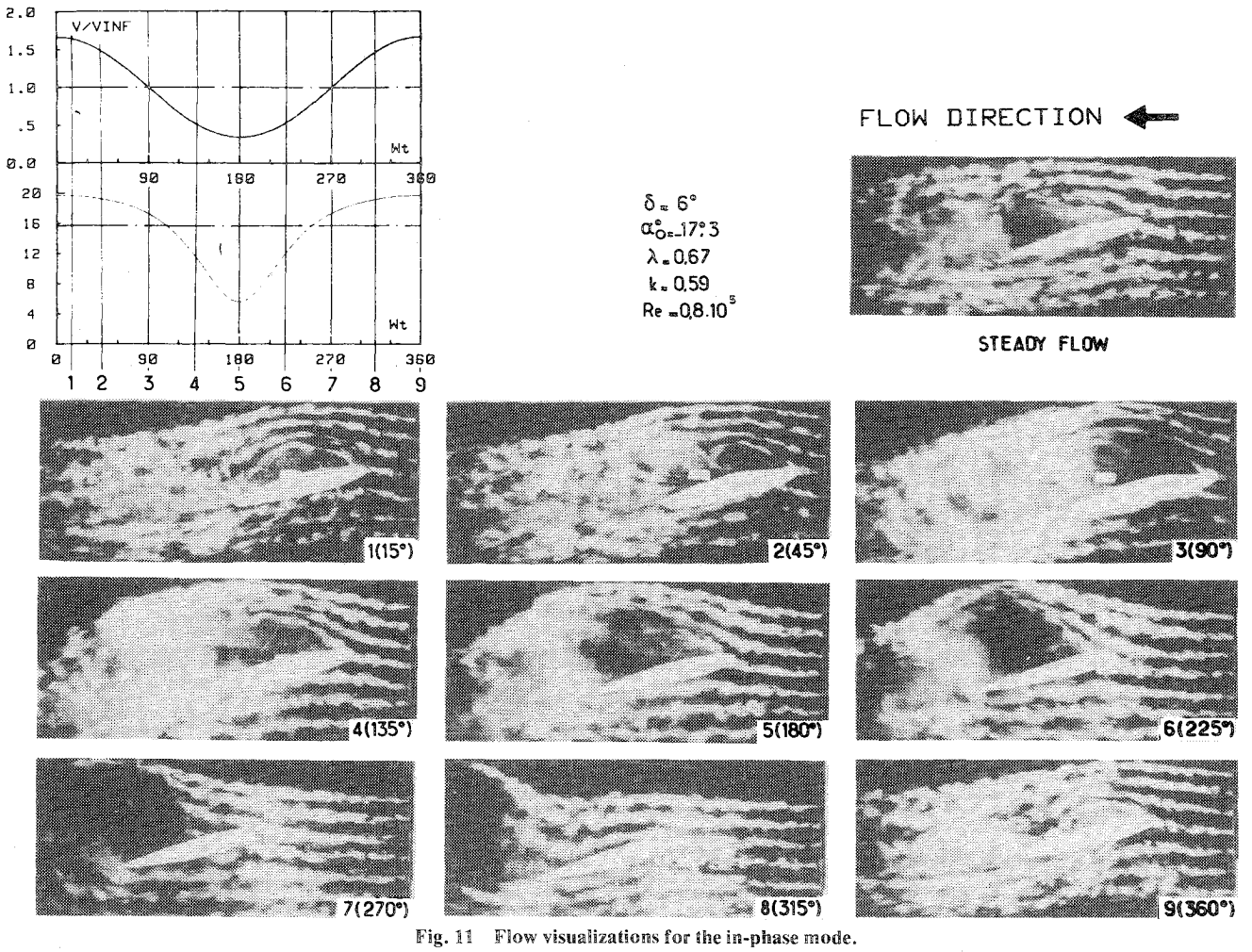

Fig. 11 Flow visualizations for the in-phase mode.

Oscillation through Dynamic Stall

Out-of-phase and in-phase variations of V and α are generated around the airfoil as shown in Fig. 2b for $\delta = 6$ deg. In each case the α oscillation varies the instantaneous incidence from $\alpha_{min} < \alpha_{SS}$ to $\alpha_{max} > \alpha_{SS}$, with an amplitude of fluctuating velocity of 67%. Corresponding results on the C_L, C_D, and C_M coefficients are given in Figs. 7-9 and are also compared to their typical quasisteady counterparts.

When out-of-phase variations of V and α (dotted lines) are simulated, hysteresis loops appear on the aerodynamic coefficients and behave in the same manner as the α oscillation (see Fig. 2b). For α increasing to α_{SS} the C_L, C_D, and C_M coefficients present variations nearly close to their quasisteady counterparts. As α is increased above α_{SS}, all of the lift, drag, and moment values increase well above the steady ones, reaching their maximum near α_{max} and then decreasing as α is decreasing.

Such unsteady behavior corroborates the well-known stall delay process previously noticed when simulating pure α oscillation due to plunging[10,15] and pitching[16,17] motions of the airfoil. Recent results[15,18] have shown that the stall phenomenon generated by the plunging and pitching motions appear to be similar, at least when the oscillation of instantaneous incidence is large enough to produce a "deep stall" (e.g., large amplitude of fluctuations $\Delta\alpha$ around a sufficiently high mean incidence α_0). In both cases, the flow separation accompanying a strong rolling-up vortex on the upper side surface generates the dynamic stall at an instantaneous incidence α_{DS} higher than α_{SS}. An abrupt fall in the aerodynamic coefficients occurs during vortex propagation until boundary-layer reattachment takes place at low incidences.

From results shown in Figs. 7-9, this typical behavior is still valid for the out-of-phase coupling case. As for a pitching or plunging airfoil, the stall delay $(\alpha_{DS} - \alpha_{SS})$ appears to be approximately equal to the amplitude of the α oscillation and no gain of the mean lift coefficient is observed over the cycle. As an example, Fig. 7 indicates that $\overline{C_L} = 0.767$, while under steady-flow conditions, the lift values obtained at α_0 and $\bar{\alpha}$ are 0.678 and 0.770, respectively.

However, during the half-period corresponding to decreasing values of α, the amount of hysteresis loops generated with pure α oscillation of the airfoil is deeper than the results shown in Figs. 7-9 for the out-of-phase coupling of V and α. As revealed by the following pressure and skin friction measurements, these different hysteresis loops can be considered to be a result of the fluctuating velocity influence, which generates a milder dynamic stall due to a different separation process on the upper side surface.

When in-phase variations of V and α are simulated (full lines), the results in Figs. 7-9 show that efforts and moment loops behave as a V oscillation (see Fig. 2b). In this case of coupling, the major effect is shown to be large amplitude fluctuations of forces and moment coefficients, with a sharp increase of the unsteady mean value over the period. For the oscillating conditions of Fig. 7, the ratio of mean unsteady lift/steady lift reaches the value $\overline{C_L}/(C_L)_{\bar{\alpha}} = 2.66$. Similar overshoots of the mean unsteady drag and moment can also be observed on Figs. 8 and 9 [$(\overline{C_D}/(C_D)_{\bar{\alpha}} = 5.2$ and $\overline{C_M}/(C_M)_{\bar{\alpha}} = 11.3$].

This favorable effect of unsteadiness on the mean lift coefficient has been previously pointed out[7,8] to be the major unsteady effect due to either the fore-and-aft motion of the airfoil or the pulsation of flow velocity around the airfoil at

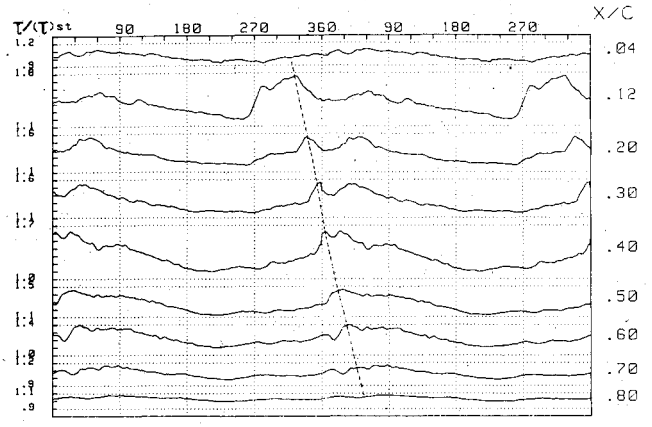

Fig. 12a Waveforms of skin friction for the in-phase mode, upper side.

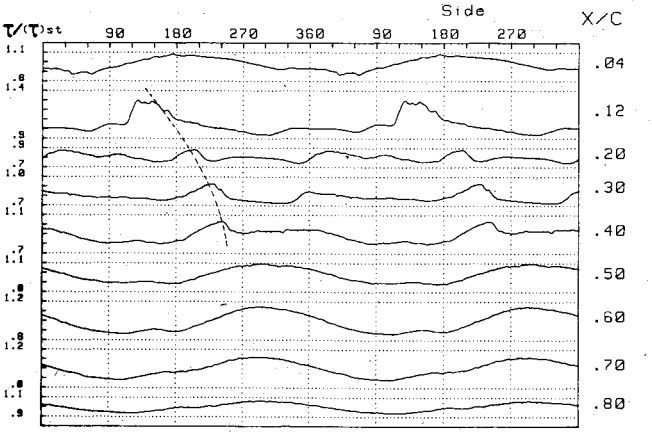

Fig. 13a Waveforms of skin friction for the out-of-phase mode, upper side.

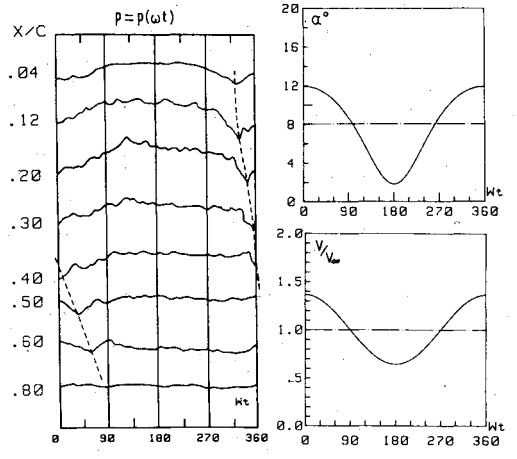

Fig. 12b Waveforms of static pressure for the in-phase mode, upper side.

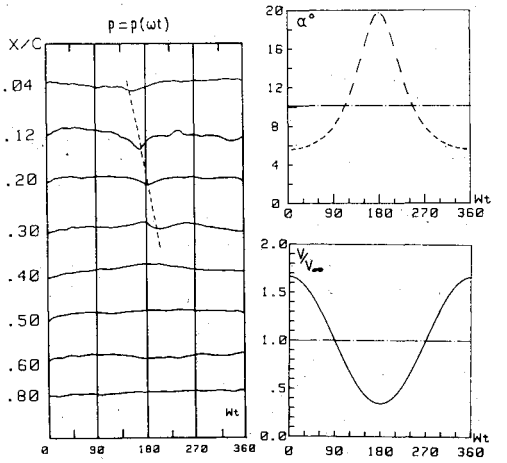

Fig. 13b Waveforms of static pressure for the out-of-phase mode, upper side.

rest. For this single V oscillation the mean lift overshoot is obtained as a result of a cyclic boundary-layer separation and reattachment phenomenon on the upper side surface. Separation occurs during the deceleration period, giving rise to a strong vortex shedding system, while dynamic reattachment observed at very high geometric incidence ($\alpha_0 = 20$ deg) takes place during the accelerated motion. Moreover, the mean lift overshoot obtained in the single V oscillation [$\overline{C_L}/(C_L)_{\alpha_0} = 2.6$ for $\alpha_0 = 20$ deg, $\lambda = 0.74$, and $k = 0.65$] is similar to the in-phase coupling result of Fig. 6, [$\overline{C_L}/(C_L)_{\alpha_0} = 2.8$ for $\alpha_0 = 17.3$ deg, $\lambda = 0.67$, and $k = 0.59$].

The different unsteady behavior of lift, drag, and moment previously described in either out-of-phase or in-phase variations of V and α can be explained by local instantaneous data deduced from visualizations, skin friction, and pressure measurements.

In Figs. 10 and 11, a series of photographs taken at an exposure of 1/1000 s describe the flow patterns at different phases of the period ($\omega t = 15$, 45, 90, 135, 180, 225, 270, 315, and 360 deg) when the airfoil is experiencing the two alternative couplings of V and α variations.

In Fig. 10, the incoming flow goes from left to right on each picture and the out-of-phase coupling is simulated. Each photograph is numbered 1-9, and the corresponding instantaneous velocity and incidence are represented in the bottom diagram. In steady conditions, the bottom right photograph shows that the flow is attached all along the upper side for $\alpha = \alpha_0 = 8$ deg and $V = V_\infty = 4$ m/s.

The flow patterns visualized on the instantaneous pictures 1-3 indicate that the flow remains attached for $0 < \omega t < 135$ deg. Beyond the phase $\omega t = 135$ deg, pictures 4-7 show that a boundary-layer disturbance originates in the leading-edge region and is propagating downstream with increasing incidences α. However, neither a complete separation of the flow in the sense of large-scale breakdown nor a strong vortex rolling close to the upper side is observed. As previously mentioned, this mild interaction between viscous and inviscid flow can explain the behavior of the forces and moments in Figs. 7-9 that have indicated amounts of hysteresis a lot smaller than those in the pitching airfoil during the decreasing values of α. Finally, instantaneous pictures 8 and 9 reveal that boundary-layer reattachment occurs from the leading edge at incidences lower than the one of static stall.

The in-phase coupling of V and α is simulated in Fig. 11, where the incoming flow goes from right to left in the pictures. The steady-flow pattern (bottom right picture) indicates the presence of a separated flow all along the upper side, while the instantaneous pictures 7 and 8 show that a dynamic reattachment occurs in a brief part of the period when the airfoil is going forward in accelerated motion. After this reattachment at very high instantaneous incidence, the growing and the bursting of a leading-edge bubble (pictures 9 and 1) give rise to a strong vortex-shedding process along the upper surface (pictures 2-4). Although lower incidences are reached near $\omega t = 180$ deg, the flow remains separated as shown on photographs 5 and 6. The occurrence of this

dynamic reattachment at an instantaneous incidence higher than α_{SS} has been already pointed out[7,8] as a pure unsteady effect due to the single V-oscillation influence.

Concerning the upper surface of the airfoil, Fig. 12 gives the time histories of skin friction τ/τ_{st}, measured along the chordwise direction from $x/c=0.04$-0.8 and for two consecutive periods of the out-of-phase or in-phase oscillations.

For the in-phase coupling of V and α (Fig. 12a), the waveform of skin friction obtained at $x/c=0.12$ presents a maximum value near $\omega t=305$ deg, indicating that the vortex has been shed and is rolling downstream as shown by successive maxima obtained on the subsequent waveform stations for $0.12<x/c<0.8$. This rolling vortex phenomenon along the upper surface is well confirmed by the time histories of static pressure, presented in Fig. 12b for one period of oscillation. The successive suction peaks observed on each waveform of $x/c=0.04$-0.7 clearly show the vortex displacement in the region of the highest incidence and velocity ($\omega t=360$ deg). From these waveforms of pressure and skin friction, the vortex appears to be convected downstream with a speed of propagation of about 45% of V_∞. It can be seen that similar values for the vortex propagation velocity are obtained when simulating only single fluctuations of velocity or incidence (see Refs. 2, 4, 7, 13, and 19).

For the out-of-phase coupling of V and α (Fig. 13a), the waveforms of τ/τ_{st} also indicate the appearance of a vortex-like disturbance in the leading-edge region ($x/c<0.04$) and for the highest incidence near $\omega t=180$ deg. However, the propagation of this disturbance has not yet been observed on the hot-film gages located behind the $x/c=0.4$ abscissa. This result is confirmed by the pressure time histories of Fig. 13b and indicates a mild interaction between viscous and inviscid flow when out-of-phase variations of V and α are simulated.

Conclusion

From the experimental results described in this paper, several different flow features can be outlined when simulating either out-of-phase or in-phase coupling of V and α by means of an oblique oscillation of the airfoil.

For an α oscillation below the angle of static stall, amplitude velocity λ, and frequency parameters k of moderate magnitude, the unsteady effects are weak and the quasisteady behavior of the forces and moment are produced when out-of-phase coupling is simulated. An increase in the mean values over the period of $\overline{C_L}$, $\overline{C_D}$, and $\overline{C_M}$ and the large amplitude fluctuations of instantaneous lift, drag, and moment are observed during the in-phase coupling of V and α.

For an α oscillation through stall, the unsteady effects are strong and the dynamic stall occurs in each simulation of coupling in-phase or out-of-phase of V and α. However, two points have to be considered:

1) When in-phase variations of V and α are simulated the V oscillation is predominant during dynamic stall. The main unsteady effect consists of an overshoot of the mean lift, drag, and moment coefficients over the period. This effect has already been pointed out as the characteristic phenomenon occurring when single fluctuations of velocity are simulated around the airfoil. The overshoots of mean aerodynamic coefficients are due to a cyclic separation/reattachment process on the upper side flow, which produces a strong vortex originated in the leading-edge region and then convected downstream close to the upper surface. Moreover, the dynamic reattachment occurs at an instantaneous incidence larger than α_{SS}, owing to fluctuations in the velocity during the accelerated phase.

2) When out-of-phase variations of V and α are simulated, the α oscillation is predominant during dynamic stall. The major unsteady feature consists of the time delay $(\alpha_{DS}-\alpha_{SS})$ obtained between incidences of dynamic and static stall, which induces hysteresis loops on the C_L, C_D, and C_M coefficients. To some extent, such typical hysteresis phenomena are similar to those obtained when single fluctuations of incidence are generated from pitching or plunging motions. However, for the out-of-phase coupling a mild separation flow process occurs on the upper side and produces a smaller amount of hysteresis on forces and moments during the decreasing phase of α. Moreover, the reattachment occurs as a quasisteady phenomenon at an instantaneous incidence lower than the angle of static stall.

Acknowledgment

This work was supported by the Service Technique des Programmes Aéronautiques under Grant 80-95025.

References

[1] McCroskey, W. J., "Some Current Research in Unsteady Fluid Dynamics," 1976 Freeman Scholar Lecture (ASME), *Journal of Fluids Engineering*, Vol. 12, March 1977, pp. 8-39.

[2] Philippe, J. J., "Le décrochage dynamique: un exemple d'interaction forte entre écoulements visqueux et non-visqueux," *AGARD-FDP on Unsteady Aerodynamics*, AGARD CP 227, Sept. 1977, Paper 21.

[3] McCroskey, W. J., Carr, L. W., and McAlister, K. W., "Dynamic Stall Experiments on Oscillating Airfoils," AIAA Paper 75-125, Jan. 1975; also *AIAA Journal*, Vol. 14, Jan. 1976, pp. 57-63.

[4] Carr, L. W., McAlister, K. W., and McCroskey, W. J., "Analysis of Dynamic Stall Based on Oscillating Airfoil Experiments," NACA TN D-8382, Jan. 1977; also NASA TP-1100, Jan. 1978.

[5] Ericsson, L. E. and Reding, J. P., "Quasi-steady and Transient Dynamic Stall Characteristics," AGARD CP 204, Feb. 1977, Paper 24.

[6] Ham, N. D. and Garelick, M. S., "Dynamic Stall Considerations in Helicopter Rotor," *Journal of American Helicopter Society*, Vol. 13, April 1968, pp. 49-55.

[7] Rebont, J., Maresca, C., Favier, D., and Valensi, J., "Recollement dynamique sur un profil d'aile en mouvement de tamis: influence des paramètres d'oscillation," *AGARD-FDP on Unsteady Aerodynamics*, AGARD CP 227, Sept. 1977, Paper 29.

[8] Maresca, C., Favier, D., and Rebont, J., "Experiments on an Aerofoil at High Incidence in Longitudinal Oscillations," *Journal of Fluid Mechanics*, Vol. 92, Pt. 4, 1979, pp. 671-690.

[9] Favier, D., Maresca, C., and Rebont, J., "Profil d'aile à grande incidence en mouvement de pilonnement," *Proceedings of 16th Colloquium of Applied Aerodynamics*, Association Aéronautique et Astronautique de France, Nov. 1979, pp. 1-21.

[10] Favier, D., "Aérodynamique instationnaire d'un profil d'aile soumis a des variations de vitesse et d'incidence," Thèse de Doctorat d'Etat, Université d'Aix-Marseille, France, Oct. 1980.

[11] Ericsson, L. E. and Reding, J. P., "Dynamic Stall Simulation Problems," *Journal of Aircraft*, Vol. 8, July 1971, pp. 579-583.

[12] Ericsson, L. E. and Reding, J. P., "Unsteady Airfoil Stall: Review and Extension," *Journal of Aircraft*, Vol. 8, Aug. 1971, pp. 609-616.

[13] Parker, A. G., "Force and Pressure Measurements on an Airfoil Oscillating through Stall," *Journal of Aircraft*, Vol. 13, Oct. 1976, pp. 823-827.

[14] Parker, A. G., "Use of Slotted Walls to Reduce Wind-Tunnel Boundary Corrections in Subsonic Flow," *AIAA Journal*, Vol. 12, Dec. 1974, pp. 1771-1772.

[15] Maresca, C., Favier, D., and Rebont, J., "Unsteady Aerodynamics of an Airfoil at High Angle of Incidence Performing Various Linear Oscillations in a Uniform Stream," *Journal of American Helicopter Society*, Vol. 26, April 1981, pp. 40-45.

[16] McCroskey, W. J. and Pucci, S. L., "Viscous-Inviscid Interaction on Oscillating Airfoils," AIAA Paper 81-0051, Jan. 1981.

[17] McCroskey, W. J., McAlister, K. W., Carr, L. W., Pucci, S. L., Lambert, O., and Indergand, R. F., "Dynamic Stall on Advanced Airfoil Sections," *Journal of American Helicopter Society*, Vol. 26, July 1981, pp. 40-50.

[18] McCroskey, W. J., "The Phenomenon of Dynamic Stall," NASA TM-81264, March 1981.

[19] Werle, H. and Armand, C., "Mesures et visualisations instationnaires sur les rotors," ONERA, Paris, TP-156, 1974.